Volume 36
Number 4
April 2021
Pages 687–858

JAAS

Journal of Analytical Atomic Spectrometry

rsc.li/jaas

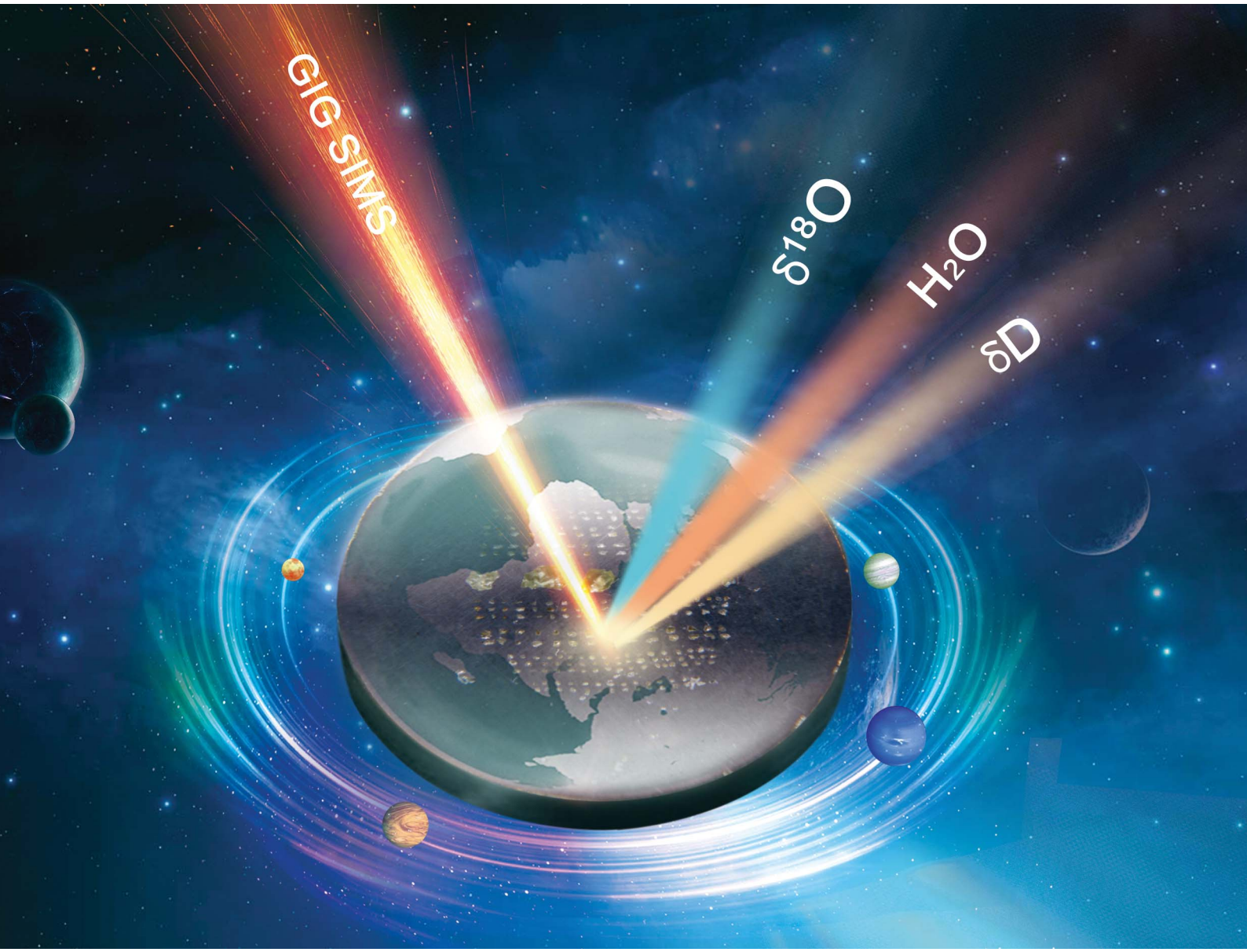

ISSN 0267-9477

ROYAL SOCIETY OF CHEMISTRY

TECHNICAL NOTE

Xiao-Ping Xia *et al.*

SIMS simultaneous measurement of oxygen–hydrogen isotopes and water content for hydrous geological samples

JAAS

ROYAL SOCIETY OF CHEMISTRY

TECHNICAL NOTE

View Article Online
View Journal | View Issue

Cite this: *J. Anal. At. Spectrom.*, 2021, **36**, 706

SIMS simultaneous measurement of oxygen–hydrogen isotopes and water content for hydrous geological samples†

Qing Yang,[ab] Xiao-Ping Xia, *[ab] Ze-Xian Cui,[ab] Wan-Feng Zhang, [ab] Yan-Qiang Zhang[ab] and Chun-Kit Lai[c]

In this study, we developed two new SIMS (secondary ion mass spectrometry) analytical protocols to simultaneously measure oxygen–hydrogen (O–H) isotopic compositions and water content for hydrous geological samples. These two protocols involve the measurement of two sets of secondary ion contents: (1) ^{1}H, ^{2}H, ^{16}O, ^{18}O; and (2) ^{16}O, $^{16}O^{1}H$, ^{18}O, $^{17}O^{1}H$, $^{16}O^{2}H$. Both measurements utilize a hybrid dynamic multi-collector system of CAMECA IMS 1280-HR, which benefits from both the static multi-collector mode and peak-hopping mono-collector mode. These new methods can simultaneously measure (with high-precision) the $^{18}O/^{16}O$ ratio in static multi-collector mode without trading off its analytical precision, and $^{1}H/^{16}O$ (or $^{16}O^{1}H/^{16}O$) and $^{2}H/^{1}H$ (or $^{16}O^{2}H/^{16}O^{1}H$) ratios in conventional peak-hopping mono-collector mode. Three glass samples (LBS7H, LBS5H and LBS6H-) with known water contents and two apatite samples (Kovdor, Durango) with known oxygen–hydrogen isotopes and water content were measured to verify the protocols' reliability. The olivine crystal San Carlos with ~1 ppmw water content was used for background monitoring. For the apatite samples, the external precision (spot-to-spot reproducibility) for $\delta^{18}O$ and δD is better than 0.56‰ (2SD) and 54‰ (2SD), respectively. After eliminating the outlier (beyond 3SD error), the external precision of $^{16}O^{1}H/^{16}O$ or $^{1}H/^{16}O$ ratio improves to 10.27% (2SD). For the glass samples, the water content calibration curves, which were constructed by comparison of the known water content with the SIMS measured $^{16}O^{1}H/^{16}O$ or $^{1}H/^{16}O$ ratios, yielded good correlations. It is noteworthy that the apatite and glass samples can have a uniform water content calibration curve for protocol 1, but not for protocol 2, indicating different matrix effects for the two protocols.

Received 27th January 2021
Accepted 11th February 2021

DOI: 10.1039/d1ja00031d

rsc.li/jaas

1. Introduction

Water, even present in trace amounts, is critical for many Earth's processes. It can alter the physicochemical properties of rocks and minerals, such as their seismic velocity, rheology, electrical conductivity, optical properties, melting temperature and ion diffusion behavior.[1–5] Therefore, understanding water content distribution and its evolution in different reservoirs is an essential part of geoscience research. Hydrogen is the most abundant element in the solar system. Since hydrogen is the lightest element, it has the largest mass-dependent fractionation in physicochemical processes, leading to an extremely wide D/H range depending on the origin of geological samples and their evolution experience.[6–8] Oxygen is the most abundant element on Earth and the main rock-forming component. Oxygen isotopes often bear the signature of geodynamic processes experienced by rocks (or minerals), and have been proven highly useful in the fields of paleo-environmental/-climatic reconstruction, detrital provenance analysis and igneous/metamorphic petrogenesis.[9–11] Therefore, measurements of water content and hydrogen–oxygen isotopes for geological samples can yield both the amount and nature (origin and evolution) of the contained water. For example, an integrated study of water content and oxygen–hydrogen isotopes of granitic rocks can provide information on the nature of their magma source and possible volcanic degassing during the magma evolution.[12,13]

Since the 1980s, the SIMS (Secondary Ion Mass Spectrometry, also called the ion microprobe) technique has been increasingly employed in earth science research, notably for *in situ* hydrogen–oxygen isotope compositions and water content micro-analysis.[6,7,14–19] Hu *et al.*[15] measured water content and hydrogen isotopes in apatite and glass samples using a Nano-SIMS. Métrich *et al.*[7] measured water content and hydrogen isotopes in mono-collection mode by high-resolution SIMS (HR-SIMS). Neither of these methods can measure oxygen isotopes

[a]*State Key Laboratory of Isotope Geochemistry, Guangzhou Institute of Geochemistry, Chinese Academy of Sciences, Guangzhou 510640, China. E-mail: xpxia@gig.ac.cn*
[b]*CAS Center for Excellence in Deep Earth Science, Guangzhou, 510640, China*
[c]*Faculty of Science, University Brunei Darussalam, Gadong BE1410, Brunei Darussalam*

† Electronic supplementary information (ESI) available. See DOI: 10.1039/d1ja00031d

at the same time. Recent studies showed that HR-SIMS can simultaneously determine water content and oxygen isotopes,[17,20] but no hydrogen isotopes were simultaneously measured. Therefore, establishing analytical protocols for simultaneous measurement of hydrogen–oxygen isotopes and water content is necessary to ensure these three sets of data to be derived from the same part of the analyzed sample, which is important for geological samples as they are often compositionally heterogeneous (*e.g.*, with the inherited core or growth rim).

In this work, we introduce two modified analytical protocols to simultaneously determine water content, and oxygen–hydrogen isotope compositions using a CAMECA IMS 1280-HR. These protocols can yield $\delta^{18}O$, δD and water content results with external precision (spot-to-spot reproducibility) better than 0.56‰ (2SD), 54‰ (2SD) and 10.27% (2RSD), respectively, for hydrous geological samples. This increases the HR-SIMS efficiency and avoid decoupling of the three datasets. Previous studies aimed at obtaining either the water content and hydrogen isotopes[7] or only hydrogen isotopes,[8] with a casting time of 16 or 20 minutes. Our modified analytical protocols can shorten the analytical time (for all three datasets) to 12 minutes.

2. Samples and sample preparation

Three glass (LBS7H, LBS5H and LBS6H-),[21] two apatite (Kovdor and Durango)[6,15,16,22,23] and one olivine (San Carlos)[15,24–26] samples were chosen for this study (Table 1). The internal structure and major element compositions of apatite minerals were previously obtained by electron probe microanalysis.[15,16,21,23] Both apatites are homogeneous in major elements (Table 1), although tiny inclusions and cracks are present. The three glass samples have been described in detail by Lin *et al.*[21] Both glasses LBS7H and LBS6H are synthesized at 1200 °C and 0.4 GPa, with H_2O (in the form of both hydroxyl and water molecules, revealed by FTIR analysis) contents of 5.7 and 1.9 mg g^{-1}, respectively.[21] Glass LBS5H is synthesized at 1200 °C and 0.8 GPa, and has 3.2 mg g^{-1} water.[21] Apatite Kovdor is collected from the Paleozoic Kovdor massif (Russia), with $\delta^{18}O = 6.55 \pm 0.38‰$ (2SD), water content = 9.8 mg g^{-1}, and $\delta D = -66 \pm 21‰$.[15,16,23] Apatite Durango comes from the Cerro de Mercado Fe deposit (Mexico). The same fragment of this Durango sample has been used for SIMS $\delta^{18}O$[16] and NanoSIMS δD and water content[15] measurements. The apatite has recommended $\delta^{18}O = 9.80 \pm 0.25‰$ (2SD), water content = 0.478 mg g^{-1}, and $\delta D = -120 \pm 5‰$.[6,15,22] The olivine San Carlos (Arizona, USA) is commonly used to calibrate SIMS $\delta^{18}O$ measurements, and has a recommended $\delta^{18}O$ of 5.27 ± 0.04‰ (2SD) and a water content of 0.001 mg g.[15,24–26]

All the samples were placed on a double adhesive tape and enclosed in a Sn-based alloy (52% Sn + 48% Bi), according to the method described by Zhang *et al.*[27] The alloy has a melting point of ~90 °C and a Brinell hardness of 20. It is used to replace epoxy resins in order to avoid continuous hydrocarbons and water degassing under vacuum conditions and achieve low water background. The Sn-based alloy mount was photographed under reflected light microscopy, and then vacuum-coated with high-purity gold to yield <20 Ω resistance across the mount surface to prevent the charging effect during SIMS analysis. Before the analysis, the prepared mount was placed into the storage chamber of IMS 1280-HR overnight under high vacuum conditions (~1×10^{-8} mbar), with the aim of further reducing water background.

3. Analytical methods

For the analysis, the CAMECA IMS 1280-HR instrument was used at the SIMS Laboratory of Guangzhou Institute of

Table 1 Descriptions of the samples used in this study

Sample	Kovdor	Durango	LBS5H	LBS6H-	LBS7H	San Carlos
Description	Kovdor apatite, Russia	Durango apatite, Mexico	Glass, synthetic	Glass, synthetic	Glass, synthetic	San Carlos olivine, USA
H_2O (mg g^{-1})	9.8	0.478	3.2	1.9	5.7	0.001
$\delta D‰^{a}$	−66 ± 21	−120 ± 5	—	—	—	—
$\delta 18O‰^{b}$	6.55 ± 0.38	9.80 ± 0.25	—	—	—	5.27 ± 0.04
SiO_2	0.64	0.21	48.05	48.72	49.14	41.32
TiO_2	0.00	0.00	1.67	2.33	2.13	—
Al_2O_3	0.00	0.00	14.80	16.62	15.82	—
FeO	0.01	0.05	12.81	12.68	11.61	8.8
MgO	0.01	0.02	10.59	7.26	7.59	49.89
CaO	53.46	53.59	10.60	11.44	11.9	0.06
P_2O_5	40.45	41.19	—	—	—	—
F	0.36	3.41	—	—	—	—
Cl	0.01	0.41	—	—	—	—
Na_2O	0.07	0.26	—	—	—	—
MnO	0.01	0.01	—	—	—	0.13
SO_3	0.01	0.10	—	—	—	—
Total mass	94.87	97.72	98.52	99.05	98.19	100.20
References	15, 16, and 23	6, 15, and 16	21	21	21	15 and 24–26

[a] Average ± 2SD, $\delta D = [(D/H)\text{ sample}/(D/H)\text{ VSMOW} - 1] \times 1000$, where VSMOW is the Vienna standard mean ocean water with a D/H ratio of 1.5576×10^{-4}. [b] Average ± 2SD, $\delta^{18}O = [(^{18}O/^{16}O)\text{ sample}/(^{18}O/^{16}O)\text{ VSMOW} - 1] \times 1000$, where VSMOW is the Vienna standard mean ocean water with a $^{18}O/^{16}O$ ratio of 2.0052×10^{-3}.

Geochemistry, Chinese Academy of Sciences (GIGCAS). The instrument is a large-geometry, double-focusing mass spectrometer equipped with both mono- and multi-collector systems (Fig. 1a). The multi-collector system consists of seven motorized detectors, which are movable along the focal plane to optimize the collection of different masses. The mass resolving power (MRP) is fixed at 2400, 4800, or 8000 (50% peak height definition hereafter). The multi-collector system is commonly used for high-precision measurement of multiple masses, with the maximum mass dispersion and minimum mass gap being approximately 17% and 0.4% of the axial mass, respectively. The mono-collector system is installed independently outside the focal plane, which allows a very high MRP of up to ~40 000. The mono-collector system is commonly used for simultaneous determination of different masses, in the peak-hopping mode by changing magnet settings. In this study, we developed two hybrid "dynamic multi-collector" analytical protocols for high-precision measurement of $^{18}O/^{16}O$ ratios (using the multi-collector system) and ^{1}H, ^{2}H or $^{16}O^{1}H$, $^{16}O^{2}H$ (using the mono-collector system), which have a large mass dispersion or require very high MRP (~15 000), respectively.

3.1. Protocol 1

A primary Cs^{+} beam (3.9–4.3 nA) was accelerated at 10 kV and focused in Gaussian mode to sputter the samples. A 15 μm raster was applied to ensure a more uniform flat-bottom sputter crater. A normal-incidence electron gun was used to ensure charge compensation and to maintain voltage stability. Negative secondary ions were extracted and accelerated through a 10 kV potential with a 400 μm contrast aperture. The energy slit was closed to a bandwidth of 50 eV width and shifted 5 eV below the maximum transmission. A 120 μm entrance slit, 600 μm exit slit, and 100× transfer optical magnification were used to guide the secondary ions. To minimize the water background signal, a 2000 μm field aperture (FA) was used and $<3 \times 10^{-9}$ mbar vacuum was obtained in the sample chamber.

^{1}H, ^{2}H, ^{16}O and ^{18}O signals were measured in a single acquisition (Fig. 1b). In this protocol, the Faraday cup (FC) with

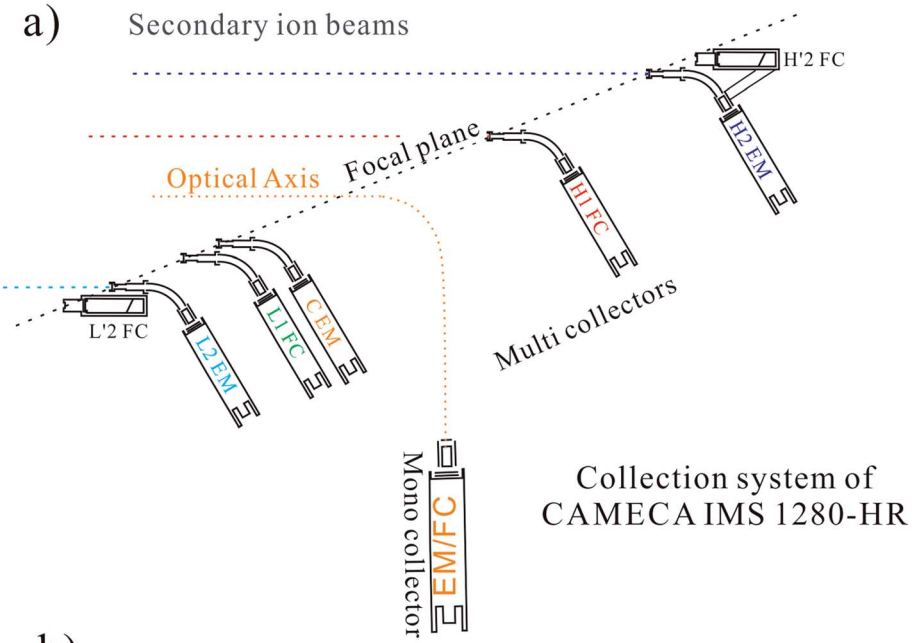

b)

	Step	Species in Detectors			Waiting time (s)	Counting time (s)
		L'2	Axial detector	H1		
Protocol 1	1		^{1}H (FC2)		6	4
	2		^{2}H (EM)		0.96	4
	3	^{16}O		^{18}O	3.12	4
	Step	Species in Detectors			Waiting time (s)	Counting time (s)
		L'2	Axial detector	H2		
Protocol 2	1	^{16}O	$^{16}O^{1}H$ (EM)	^{18}O	2	4
	2		$^{17}O^{1}H$ (EM)		1.04	4
	3		$^{16}O^{2}H$ (EM)		1.04	6

Fig. 1 (a) Schematic diagram of the CAMECA IMS 1280-HR collection system. The detectors L2, C, and H2 are equipped with EMs, and the detectors L′2, L1, H1, and H′2 with FCs. The axial detector is equipped with an EM and two FCs, which is selected based on the content of the analysis object (modified after Liu *et al.*[33]). (b) The detector configuration of these two protocols.

a resistor of 10^{11} Ω of the mono-collector system was used to detect ^{1}H, and the electron-multiplier (EM) of the mono-collector system was used to detect ^{2}H ions. Two movable Faraday cups of the multi-collector system (L′2 and H1), with resistors of 10^{10} Ω and 10^{11} Ω, respectively, were used to detect ^{16}O and ^{18}O ions. In this protocol, 2000 and 2400 MRP was used for the mono- and multi-collector system, respectively. The collector configuration is shown in Fig. 1b, and the data acquisition comprises three sequences. ^{1}H and ^{2}H were measured during the first and secondary sequence, whilst ^{16}O and ^{18}O were measured simultaneously on L′2 and H1 during the third sequence. The counting time for each sequence was 4, 4, and 4 s, and the waiting time was 6, 0.96, and 3.12 s, respectively. Before the data acquisition (for both protocol 1 and 2), each spot was sputtered pre-analysis for 100 s using a 25 μm square raster to remove the gold coating and to minimize the water background. The secondary ions were centered in the field aperture and the entrance slit by scanning the peak of ^{16}O in detector L′2 to ensure similar conditions for each analysis. Peak centering was performed before each analysis by centering the peak of ^{16}O in detector L′2. Each measurement consists of 16 cycles, and the total analytical time is about 12 min. In this protocol, the water content was calibrated with the relative signal intensity of ^{1}H to ^{16}O.

3.2. Protocol 2

Most instrument setting parameters for protocol 2 were identical to those for protocol 1. Only those different were described here in detail. Negative secondary ions were extracted and accelerated through a 10 kV potential with a 400 μm contrast aperture, entrance slit of 20 μm, exit slit of 80 μm, 50 eV energy width (with a 5 eV offset), and transfer optics magnification of 100×. Such aperture settings are different from those of protocol 1 in order to achieve 15 000 MRP in the mono-collector system to completely separate $^{17}O^{1}H$ from $^{16}O^{2}H$ with sufficient flat-topped peaks.[7]

The ^{16}O, $^{16}O^{1}H$, ^{18}O, $^{17}O^{1}H$, $^{16}O^{2}H$ signals were determined in a single acquisition (Fig. 1b). In this protocol, 2400 and 15 000 MRP were used for the multi- and mono-collector system, respectively. Acquisition was divided into 3 sequences. The ^{16}O, $^{16}O^{1}H$ and ^{18}O were measured simultaneously on L′2, the mono-collector and H1 during the first sequence, similar to the static multi-collector configuration.[17] The $^{17}O^{1}H$ and $^{16}O^{2}H$ were measured using the mono-collector during the second and third sequences, respectively. The EM of the mono-collector system was used to detect the $^{16}O^{1}H$, $^{17}O^{1}H$ and $^{16}O^{2}H$ ions. The main purpose of measuring $^{17}O^{1}H$ was to check that $^{16}O^{2}H$ was measured correctly and that $^{17}O^{1}H$ and $^{16}O^{2}H$ are completely separated. The counting time and waiting time for each step were 4, 4, 6 s and 2, 1.04, 1.04 s, respectively. As the EM gain possibly descends with time (*i.e.*, the EM attenuation effect), the EM HV adjustment and EM drift correction were routinely conducted during every measurement by using the CAMECA analysis program with the $^{16}O^{1}H$ peak. Each measurement consists of 16 cycles, and the total analysis time is about 11 min. For protocol 2, the water content was calibrated with the relative signal intensity of $^{16}O^{1}H$ to ^{16}O.

4. Results

4.1. Protocol 1

By using this protocol, a total of two SIMS measurement sessions have been conducted. Detailed $^{18}O/^{16}O$, $^{1}H/^{16}O$ and $^{2}H/^{1}H$ ratios obtained are listed in Table S1† and summarized in Table 2. Eight spots have been analyzed for each sample in each session. The standard deviations of $\delta^{18}O$ values (reference to VSMOW $^{18}O/^{16}O = 0.0020052$)[16] and δD values (reference to VSMOW $^{2}H/^{1}H = 1.5576 \times 10^{-4}$)[15] for the five samples are 0.31–0.79‰ (2SD) and 22–50‰ (2SD), respectively (Table 2). The relative standard deviations of water contents for the five samples are 2.06–7.72% (2RSD) (Table 2).

The recommended values of $\delta^{18}O = 9.80 \pm 0.25$‰ (2SD)[16,22] and $\delta D = -120 \pm 5$‰ (2SD)[15] for the Durango apatite, and $\delta^{18}O = 6.55 \pm 0.38$‰ (2SD)[16] and $\delta D = -66 \pm 22$‰ (2SD)[15] for the Kovdor apatite were used here to calculate the instrument mass fractionation (IMF):

$$IMF_O = (\delta^{18}O)_M - (\delta^{18}O)_R \text{ and } IMF_H = \delta D_M - \delta D_R$$

where the subscript "M" denotes the raw value measured by SIMS, and "R" denotes the recommended value. The IMF_O values for Kovdor and Durango are 8.50 ± 0.48‰ (2SD) and 8.30 ± 0.56‰ (2SD) in session 1, and 8.56 ± 0.31‰ (2SD) and 8.10 ± 0.34‰ (2SD) in session 2 (Table 2). The IMF_H values for Kovdor and Durango are 99 ± 22‰ (2SD) and 119 ± 50‰ (2SD) in session 1, and 134 ± 20‰ (2SD) and 155 ± 37‰ (2SD) in session 2 (Table 2).

The average measured $^{1}H/^{16}O$ ratios (Fig. 2) for the samples range from 7.15×10^{-5} (Durango) to 1.17×10^{-3} (Kovdor) in session 1, and from 7.54×10^{-5} (Durango) to 1.20×10^{-3} (Kovdor) in session 2 (Table 2). Single spot internal precision of $^{1}H/^{16}O$ ranges mainly from 0.11% (LBS5H; 2RSE) to 1.04% (Kovdor; 2RSE) in session 1, and from 0.26% (LBS5H; 2RSE) to 2.33% (LBS6H-; 2RSE) in session 2 (Table S1†).

4.2. Protocol 2

Detailed $^{18}O/^{16}O$, $^{16}O^{1}H/^{16}O$ and $^{16}O^{2}H/^{16}O^{1}H$ ratios obtained are listed in Table S1† and summarized in Table 2. In total, two sessions and seven spots in each session have been analyzed for all the samples. Standard deviations of the $\delta^{18}O$ and δD values for the all the hydrous samples in session 1 are 0.41–1.13‰ (2SD) and 21–55‰ (2SD), respectively (Table 2). The relative standard deviation of water contents is of 1.11–8.32% (2RSD) (Table 2). The IMF_O values for Kovdor and Durango are 5.08 ± 0.52‰ (2SD) and 5.11 ± 0.47‰ (2SD) in session 3, and are 4.05 ± 0.41‰ (2SD) and 4.15 ± 0.49‰ (2SD) in session 4 (Table 2). The IMF_H values for Kovdor and Durango are 523 ± 21‰ (2SD) and 530 ± 54‰ (2SD) in session 3, and 508 ± 22‰ (2SD) and 538 ± 33‰ (2SD) in session 4 (Table 2). The average measured $^{16}O^{1}H/^{16}O$ ratios for the samples range from 3.09×10^{-4} (Durango) to 6.00×10^{-3} (Kovdor) in session 3, and from 2.98×10^{-4} (Durango) to 6.20×10^{-3} (Kovdor) in session 4 (Fig. 3; Table 2). Single spot internal precision of $^{16}O^{1}H/^{16}O$ ranges mainly from 0.27% (LBS6H-; 2RSE) to 0.92% (Kovdor; 2RSE) in

Table 2 Summary of average measured $\delta^{18}O$ values, δD values and water contents[a]

Protocol	Session	Sample	Number	Uncorrected δD	IMF	2SD (‰)	Outliers number	Uncorrected $\delta^{18}O$	IMF	2SD (‰)	Outliers number	Average water content ratio ($^{1}H/^{16}O$ or $^{16}O^{1}H/^{16}O$)	2RSD (%)	Recommended[b] mg g^{-1}	Outliers number
Protocol 1	Session 1	Kovdor	8	33	99	22	0	15.05	8.50	0.48	0	1.17×10^{-3}	3.61	9.8	0
		Durango	8	−1	119	50	0	18.10	8.30	0.56	1	7.15×10^{-5}	4.57	0.478	0
		LBS5H	8	11		23	0	10.99		0.79	0	4.38×10^{-4}	3.10	3.2	0
		LBS6H-	8	−60		33	1	10.15		0.40	0	2.86×10^{-4}	2.06	1.9	1
		LBS7H	8	−78		23	0	10.25		0.79	0	8.74×10^{-4}	4.06	5.7	1
	Session 2	Kovdor	8	68	134	20	0	15.11	8.56	0.31	0	1.20×10^{-3}	3.10	9.8	0
		Durango	8	35	155	37	0	17.90	8.10	0.34	0	7.54×10^{-5}	4.36	0.478	0
		LBS5H	8	26		25	0	10.09		0.67	0	4.57×10^{-4}	4.37	3.2	0
		LBS6H-	8	−25		48	1	9.65		0.77	0	3.08×10^{-4}	4.19	1.9	1
		LBS7H	8	−53		39	1	10.41		0.67	0	8.87×10^{-4}	7.72	5.7	1
Protocol 2	Session 3	Kovdor	7	456	523	21	0	11.63	5.08	0.52	1	6.00×10^{-3}	3.27	9.8	0
		Durango	7	410	530	54	0	14.97	5.11	0.47	2	3.09×10^{-4}	1.11	0.478	0
		LBS5H	7	608		50	0	6.81		0.66	0	8.63×10^{-4}	2.25	3.2	1
		LBS6H-	7	519		30	0	8.06		0.61	0	5.49×10^{-4}	1.56	1.9	1
		LBS7H	7	481		53	0	8.02		1.00	0	1.65×10^{-3}	6.24	5.7	0
		San Carlos	7	332		309	0	7.45		0.35	0	5.15×10^{-6}	10.27	0.001	0
	Session 4	Kovdor	7	442	508	22	0	10.60	4.05	0.41	0	6.20×10^{-3}	1.58	9.8	0
		Durango	7	418	538	33	0	13.95	4.15	0.49	0	2.98×10^{-4}	3.55	0.478	0
		LBS5H	7	618		38	0	5.75		0.97	0	8.38×10^{-4}	6.62	3.2	0
		LBS6H-	7	526		53	0	7.95		0.63	0	5.47×10^{-4}	4.88	1.9	1
		LBS7H	7	473		55	0	7.46		1.13	0	1.60×10^{-3}	8.32	5.7	1

[a] All data with unexpected internal error and beyond the 3SD error were eliminated. [b] The water content data were from Hu *et al.*[15] and Lin *et al.*[21], respectively.

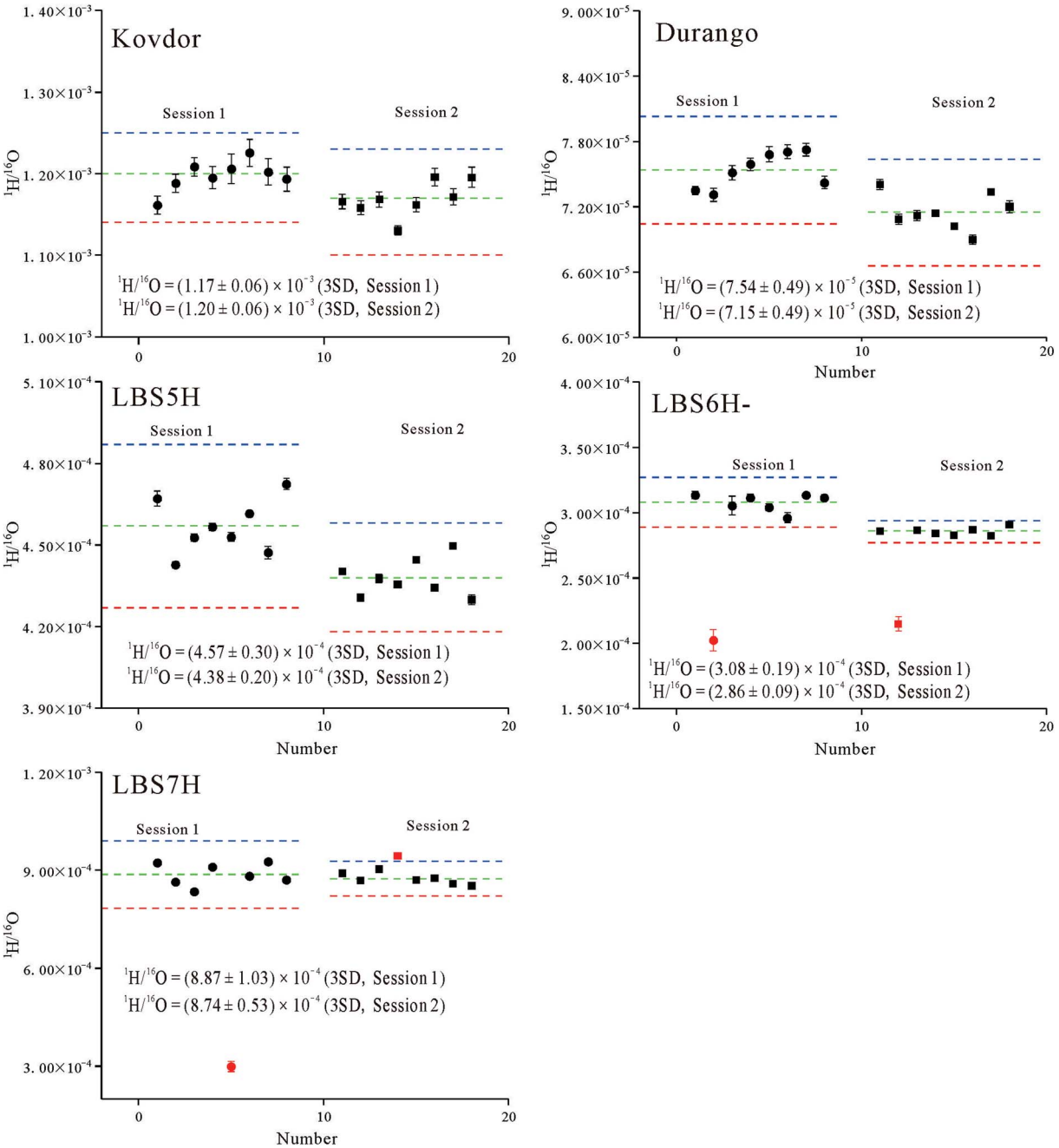

Fig. 2 SIMS analysis results of $^1H/^{16}O$ ratio in protocol 1.

session 3, and from 0.24% (LBS6H-; 2RSE) to 1.55% (LBS7H; 2RSE) in session 4 (Table S1†).

The olivine San Carlos was measured in session 3, and its average measured $^{16}O^1H/^{16}O$ ratio (Fig. 3) and relative standard deviation are 5.15×10^{-6} and 10.27% (2RSD), respectively (Table 2).

5. Discussion

Two apatite samples (Kovdor and Durango) with known hydrogen and oxygen isotope compositions are used to evaluate the accuracy and precision of isotope measurements, while all the apatite and glass samples (LBS7H, LBS5H and LBS6H-) are used to check the accuracy and uncertainty (of external calibration) of water content for the two protocols. The olivine San Carlos is used to monitor the analytical background. There are always isolated outliers for all three datasets (hydrogen and oxygen isotopes, and water content), possibly caused by water-rich micro-inclusions or micro-cracks encountered during the secondary ion sputtering. Previous hydrogen isotope[8] and oxygen isotope[11] analyses have also reported such micro-inclusions/-cracks even for gem-quality samples. Although

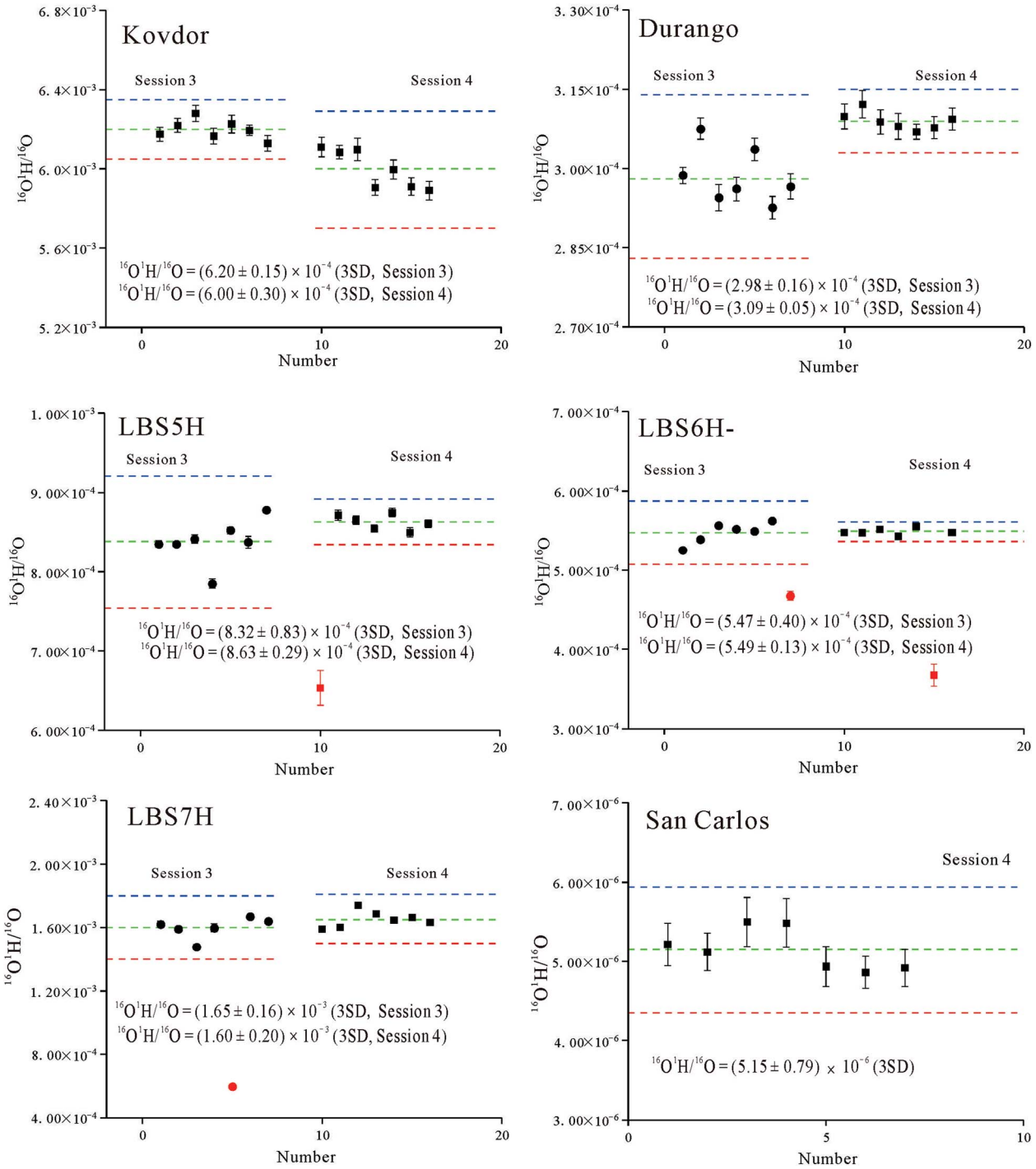

Fig. 3 SIMS analysis results of $^{16}O^1H/^{16}O$ ratio in protocol 2.

SEM images were used to choose the analytical spots here, such impurities cannot be completely avoided. Cycle-by-cycle checking of the isolated data does little help to identify any abnormal data, and the outliers are identified by statistical processing to beyond 3SD error. Some of these outliers (*e.g.*, LBS5H@1 and LBS6H-@6 in session 3) have a clearly higher ^{16}O yield, suggesting a higher oxygen impurity. These datasets were discarded from further calculation to improve the spot-to-spot external precision (Table S1†).

5.1. Analytical precision and accuracy

The analytical precision discussed here includes both internal (within-spot analysis, 2SE) and external (reproducibility) precision of spot-to-spot analysis (2SD). For the apatite oxygen isotopes, the external precision of the two protocols is <0.56‰, which is slightly higher than that achieved by previous studies (0.38‰, 2SD[16] or 0.25‰, 2SD[22]), but still acceptable in most cases when considering that oxygen isotope variation in

magmas is mostly from below 5 to over 10.[28,29] Possible reasons for the larger uncertainty include (1) the hybrid "dynamic multi-collector" mode used here cannot employ the nuclear magnetic resonance (NMR) controller, which can lock the magnet setting and enhance analytical precision in conventional SIMS oxygen isotope measurements; (2) for protocol 2, narrow apertures and slits were used to achieve high mass resolution, which significantly reduced ion transmission. The secondary ion yielded for ^{16}O is only $\sim 9 \times 10^7$ cps nA^{-1}, 10% of that yielded by conventional methods;[16] (3) in protocol 2, the ^{16}O and ^{18}O were measured using different types of detectors (FC and EM, respectively), which may degrade the analysis precision. It is noteworthy that the external precision of the two protocols is comparable, which implies that NMR is critical for high-precision isotope measurements. To evaluate the analytical accuracy for oxygen isotopes, IMF_O values were calculated for the two apatite samples, which varied from 8.10 ± 0.34 to $8.56 \pm 0.31‰$ in protocol 1 and 4.05 ± 0.41 to $5.11 \pm 0.47‰$ in protocol 2, consistent with each other within analytical uncertainties for both protocols (Table 2). This indicates that the IMF for the oxygen isotope analysis using both protocols can be accurately corrected.

For hydrogen isotopes, the external precision of the two protocols is below 54‰, similar to that on apatite hydrogen isotopes reported by Hu *et al.*[15] using NanoSIMS. The analysis for Durango (by protocol 2, session 3) yielded the largest uncertainty of about 54‰, possibly because (1) this sample has low water content (0.478 mg g^{-1}) and ^1H signal intensity; (2) ^1H is collected by FC while ^2H by EM. The IMF_H values calculated for the different analytical sessions and different apatite samples vary from 99 ± 22 to $155 \pm 37‰$ in protocol 1 and from 508 ± 22 to $538 \pm 33‰$ in protocol 2, consistent with each other within analytical uncertainties for both protocols (Table 2). This consistency demonstrates that the IMF for the hydrogen isotope analyses using both protocols can also be accurately corrected.

For the water content measurements, the precision of $^1H/^{16}O$ or $^{16}O^1H/^{16}O$ ratios for all the apatite and glass samples is better than 2.33% (internal; Table S1†). It is clear that LBS7H (session 1), LBS5H and LBS6H (session 3), and LBS6H and LBS7H (session 4) have isolated data points beyond 3SD error (red points; Fig. 2 and 3). After the removal of these isolated data points, all the hydrous apatite and glass samples have a spot-to-spot external precision better than 8.32% (external; Table 2), similar to that on the zircon water content analysis reported by Xia *et al.*[17]

5.2. Background

It is known that the water ($^{16}O^1H$ or H) background measured by SIMS is related to the residual H_2O in the vacuum. Previous studies showed that the measured background hydrogen counting rates (H_{cps})[15] or $^{16}O^1H/^{16}O$ ratios or $^1H/^{16}O$ ratios[30] correlate closely with the analysis vacuum conditions. Since epoxy mount degassing is the main contributor to poor vacuum conditions, the Sn-based alloy was used here, which achieved 2.9×10^{-9} mbar pressure in our SIMS analysis chamber (similar to the vacuum we used before[17]). In protocol 1, since we targeted the more-hydrous (>0.478 mg g^{-1}) apatite and glass for the water background measurement and chose FC as the $^1H^-$ detector, it cannot be used to measure the anhydrous olivine San Carlos (about 0.001 mg g^{-1}). In session 3, the average $^{16}O^1H^-$ of San Carlos is 1.71×10^3, which is almost two orders of magnitude lower than that of Durango (8.75×10^4). Durango has the lowest water content in all of our samples, which means that the background contribution to the sample measurement is negligible. We also used the San Carlos data as the background for the background subtraction, and the results are very similar to those from our current water content and hydrogen isotope data. Therefore, the background water content has a negligible impact on this study, yet background evaluation for more-anhydrous (<0.478 mg g^{-1}) samples is advisable.

5.3. Water content calibration

The water content calibration curves ($[H_2O] = \alpha \times [^1H/^{16}O] + \beta$ or $[H_2O] = \alpha \times [^{16}O^1H/^{16}O] + \beta$) were established by comparing the known water content with the determined SIMS $^1H/^{16}O$ or $^{16}O^1H/^{16}O$ ratios (Fig. 4). The calibration curves are regressed using the York fit method with error weighted. In both protocols 1 and 2, the blue and red solid curves are constructed based on the glass and apatite samples, respectively, while the green dotted curve incorporates both the glass and apatite samples. It is seen that the blue solid curve is plotted with $\alpha = 6258.327$ and $\beta = 0.306$, the red solid curve with $\alpha = 8500.761$ and $\beta = -0.129$, and the green dotted curve with $\alpha = 6812.377$ and $\beta = 0.004$ in session 1 (Fig. 4a). In session 2, the blue solid curve is plotted with $\alpha = 6558.984$ and $\beta = 0.051$, the red solid curve with $\alpha = 8308.522$ and $\beta = -0.148$, and the green dotted curve with $\alpha = 6811.890$ and $\beta = -0.039$ (Fig. 4b). In session 3, the blue solid curve is plotted with $\alpha = 3240.140$ and $\beta = 0.150$, and the red solid curve with $\alpha = 1638.329$ and $\beta = -0.028$ (Fig. 4c). In session 4, the blue solid curve is plotted with $\alpha = 3636.368$ and $\beta = 0.019$, and the red solid curve is plotted with $\alpha = 1580.046$ and $\beta = 0.006$ (Fig. 4d). The error bar represents 1SD. The β values in all four sessions are very small, indicating negligible water background. Regardless of the major chemical differences between apatite and glass, they share a similar calibration curve (green dotted curve) in protocol 1 (Fig. 4a and b). However, the apatite samples behave very differently from the glass samples in protocol 2, forming two different calibration curves (Fig. 4c and d). The main reason for this difference is likely attributed to the different forms of water in glass and apatite. Water occurs mainly in hydroxyl form in apatite, whereas it occurs in both hydroxyl and water molecule forms in glass.[31,32] In protocol 1, when measuring $^1H/^{16}O$, all the water-bearing species (OH in apatite, OH and H_2O in glass) would be transformed into ^1H. The ionization energies required by different kinds of samples are largely the same, and only small matrix effect is present. In contrast, when using the Cs^+ primary beam to sputter the $^{16}O^1H$ secondary ions in protocol 2, $^{16}O^1H$ is more easily sputtered for apatite than for glass, as water molecules need more energy to break and ionize. These results are similar to the findings by Hu *et al.*[15] To summarize, if the study focus is on determining the water content and no standard sample matching the target

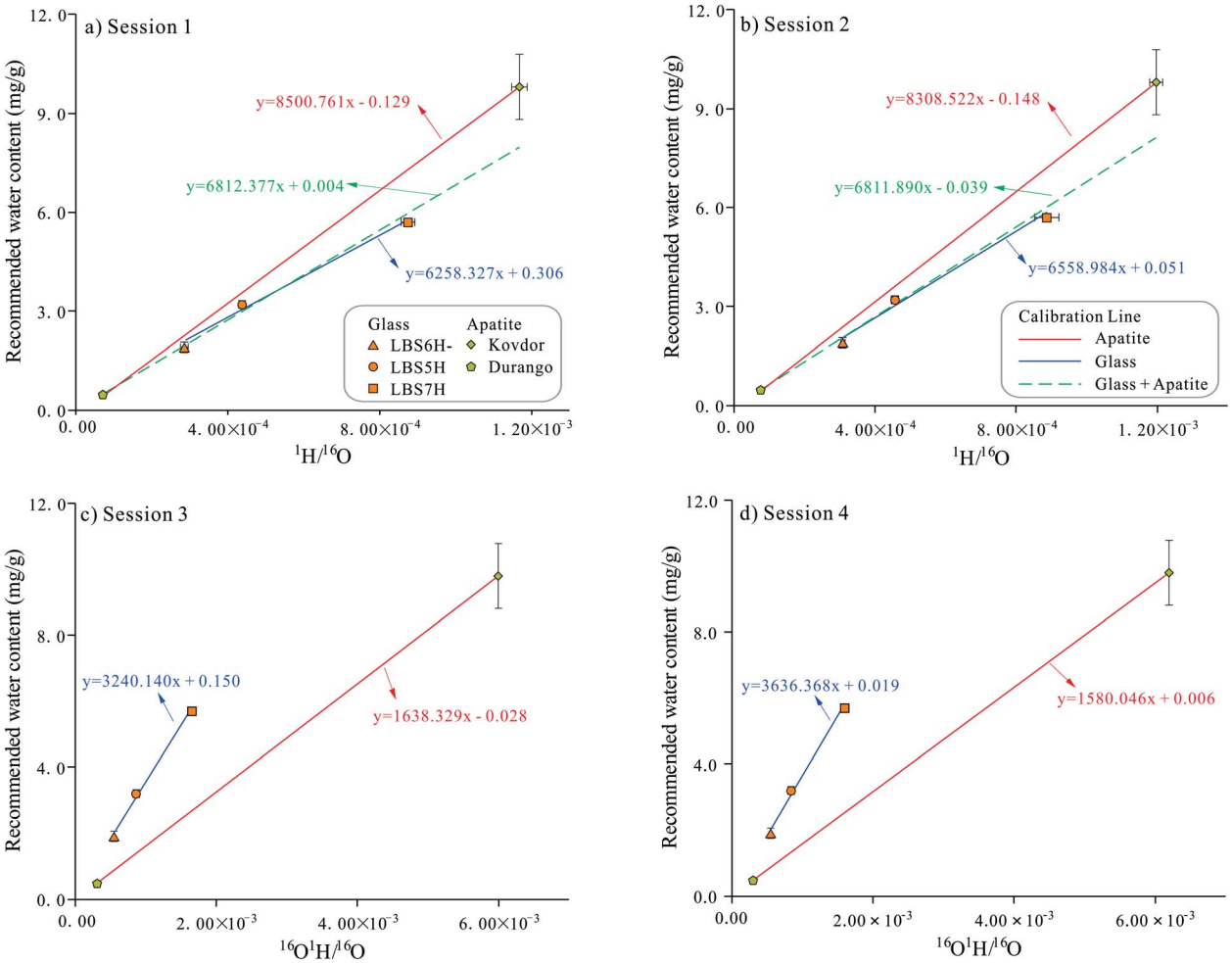

Fig. 4 Water content calibration curves for the three glass and two apatite samples. In all figures, the blue and red solid curves are constructed based on the glass and apatite samples, respectively, while the green dotted curve incorporates all the samples. (a) session 1 of protocol 1; (b) session 2 of protocol 1; (c) session 1 of protocol 2; (d) session 2 of protocol 2.

analyte matrix is available, then protocol 1 is preferred. The mass resolution of protocol 1 is lower than protocol 2, and the loss of signal is also lower. However, due to the limited range of matrix compositions investigated here, we cannot preclude that the different major element compositions in the same sample species (*e.g.*, apatite) may also have different calibration curves and worth further study.

6. Conclusions

Two hybrid "dynamic multi-collector" analytical protocols were developed with a CAMECA IMS 1280-HR to simultaneously determine the hydrogen–oxygen isotopes and water content. The external precision (spot-to-spot reproducibility) of $\delta^{18}O$ and δD values is better than 0.56‰ and 54‰ (2SD), respectively. After eliminating the outlier (beyond 3SD error), an external precision of 10.27% (2SD) can be achieved for $^{16}O^{1}H/^{16}O$ or $^{1}H/^{16}O$ ratios. Water content calibration curves were constructed by comparing the known values with the SIMS measured $^{16}O^{1}H/^{16}O$ or $^{1}H/^{16}O$ ratios. The three glass samples used for the calibration curves indicate very good correlations. Despite the major chemical difference between apatite and glass, they have similar calibration curves within the protocol 1 analytical error. For protocol 2, apatite behaves very differently from glass, indicating a marked matrix effect. We suggest that if the analysis focus is on water content and no matrix matched standard sample is available, protocol 1 is recommended.

Conflicts of interest

There are no conflicts to declare.

Acknowledgements

This work was jointly supported by the China National Key R & D Program (2018YFA0702600), State Key Laboratory of Isotope Geochemistry (SKLaBIG-JY-16-03) and NSFC (41703004 and 42077404). This is contribution No. IS-2988 from GIGCAS.

References

1 S. Karato, *Nature*, 1990, **347**, 272–273.

2 G. Hirth and D. L. Kohlstedt, *Earth Planet. Sci. Lett.*, 1996, **144**, 93–108.
3 A. M. Hofmeister, *Phys. Earth Planet. Inter.*, 2004, **146**, 483–495.
4 T. Yoshino, T. Matsuzaki, S. Yamashita and T. Katsura, *Nature*, 2006, **443**, 973–976.
5 I. Katayama and S.-I. Karato, *Phys. Earth Planet. Inter.*, 2008, **166**, 57–66.
6 J. P. Greenwood, S. Itoh, N. Sakamoto, E. P. Vicenzi and H. Yurimoto, *Geophys. Res. Lett.*, 2008, **35**, 1–5.
7 N. Métrich and E. Deloule, *Lithos*, 2014, **206–207**, 400–408.
8 A. Wudarska, M. Wiedenbeck, E. Słaby, A. Lepland, Ł. Birski and K. Simon, *Precambrian Res.*, 2018, **310**, 153–164.
9 M. S. Riishuus, C. Harris, D. W. Peate, C. Tegner, J. R. Wilson and C. K. Brooks, *Contrib. Mineral. Petrol.*, 2015, **169**(5), 41.
10 L. France, M. Demacon, A. A. Gurenko and D. Briot, *Lithos*, 2016, **260**, 328–338.
11 Q. Yang, X. Xia, W. Zhang, Y. Zhang, B. Xiong, Y. Xu, Q. Wang and G. Wei, *Solid Earth Sci. Libr.*, 2018, **3**, 81–86.
12 C. S. Wei, Y. F. Zheng and Z. F. Zhao, *Tectonophysics*, 2000, **328**, 205–227.
13 C. Francelanord, S. M. F. Sheppard and P. Lefort, *Geochim. Cosmochim. Acta*, 1988, **52**, 513–526.
14 A. M. Shaw, E. H. Hauri, T. P. Fischer, D. R. Hilton and K. A. Kelley, *Earth Planet. Sci. Lett.*, 2008, **275**, 138–145.
15 S. Hu, Y. Lin, J. Zhang, J. Hao, W. Yang and L. Deng, *J. Anal. At. Spectrom.*, 2015, **30**, 967–978.
16 Q. Yang, X. P. Xia, L. Zhang, W. Zhang, Y. Zhang, L. Chen, Y. Yang and M. He, *Surf. Interface Anal.*, 2019, **52**, 197–213.
17 X.-P. Xia, Z.-X. Cui, W. Li, W.-F. Zhang, Q. Yang, H. Hui and C.-K. Lai, *J. Anal. At. Spectrom.*, 2019, **34**, 1088–1097.
18 G. Q. Tang, B. X. Su, Q. L. Li, X. P. Xia, J. J. Jing, L. J. Feng, L. Martin, Q. Yang and X. H. Li, *Geostand. Geoanal. Res.*, 2019, **43**, 585–593.
19 J. P. Greenwood, S. Itoh, N. Sakamoto, P. Warren, L. Taylor and H. Yurimoto, *Nat. Geosci.*, 2011, **4**, 79–82.
20 M. Turner, T. Ireland, J. Hermann, P. Holden, J. A. Padrón-Navarta, E. H. Hauri and S. Turner, *J. Anal. At. Spectrom.*, 2015, **30**, 1706–1722.
21 Y. Lin, H. Hui, X. Xia, S. Shang and W. Westrenen, *Meteorit. Planet. Sci.*, 2019, **55**, 207–230.
22 J. A. Trotter, I. S. Williams, C. R. Barnes, P. Männik and A. Simpson, *Palaeogeogr., Palaeoclimatol., Palaeoecol.*, 2016, **443**, 34–48.
23 S. L. Nadeau, S. Epstein and E. Stolper, *Geochim. Cosmochim. Acta*, 1999, **63**, 1837–1851.
24 I. Ahn, J. I. Lee, M. Kusakabe and B.-G. Choi, *Geosci. J.*, 2012, **16**, 7–16.
25 C. Aubaud, A. C. Withers, M. M. Hirschmann, Y. Guan, L. A. Leshin, S. J. Mackwell and D. R. Bell, *Am. Mineral.*, 2007, **92**, 811–828.
26 W. F. Zhang, X. P. Xia, T. Eiichi, L. Li, Q. Yang, Y. Q. Zhang, Y. N. Yang, M. L. Liu and C. Lai, *Surf. Interface Anal.*, 2019, **52**, 224–233.
27 W. Zhang, X. Xia, Y. Zhang, T. Peng and Q. Yang, *J. Anal. At. Spectrom.*, 2018, **33**, 1559–1563.
28 C. J. Spencer, A. J. Cavosie, T. D. Raub, H. Rollinson, H. Jeon, M. P. Searle, J. A. Miller, B. J. McDonald and N. J. Evans, *Geology*, 2017, **45**, 975–978.
29 J. M. Eiler, *Rev. Mineral. Geochem.*, 2001, **43**, 319–364.
30 R. T. Pidgeon, A. A. Nemchin and M. J. Whitehouse, *Geochim. Cosmochim. Acta*, 2017, **197**, 142–166.
31 L. A. Silver, P. D. Ihinger and E. Stolper, *Contrib. Mineral. Petrol.*, 1990, **104**, 142–162.
32 E. Stolper, *Contrib. Mineral. Petrol.*, 1982, **81**, 1–17.
33 Y. Liu, Q.-L. Li, G.-Q. Tang, X.-H. Li and Q.-Z. Yin, *J. Anal. At. Spectrom.*, 2015, **30**, 979–985.